Analytical and Bioanalytical Chemistry (2022) 414:7325–7334
https://doi.org/10.1007/s00216-022-04284-0

RESEARCH PAPER

An ultrasensitive hairpin sensor based on g-C_3N_4 nanocomposite for the detection of miRNA-155 in breast cancer patient serum

Pingping Peng[1,2] · Sheng Wang[3] · Siyuan Cai[4] · Jing Cheng[2] · Dan Tao[5] · Nicole Jaffrezic-Renault[6] · Zhenzhong Guo[1]

Received: 3 July 2022 / Revised: 10 August 2022 / Accepted: 11 August 2022 / Published online: 16 August 2022

Abstract

Achieving the early diagnosis of breast cancer, through ultrasensitive detection of tumor marker miRNA-155, is a significant challenge. Therefore, an ultrasensitive hairpin electrochemical biosensor based on graphite-like phase carbon nitride composite was proposed. In this paper, poly(D-glucosamine) (PDG) was used as a stabilizer and reducing agent to prepare gold nanoparticles at room temperature, and then a graphite-like phase with a two-dimensional lamellar structure carbon nitride was further combined with it to obtain the poly(D-glucosamine)/gold nanoparticles/graphite-like phase carbon nitride nanocomposite (PDG/AuNPs/g-C_3N_4), in order to achieve the goal of signal amplification. The specific hairpin capture probe (HP) that recognized and bound miRNA-155 was then grafted. The hairpin biosensor showed a linear range of 0.1 fM–1 pM with a detection limit of 0.05 fM using differential pulse voltammetry (DPV) electrochemical analysis. Furthermore, the excellent performance hairpin electrochemical biosensor had been applied to the detection of miRNA-155 in human serum samples with good recovery.

Keywords Breast cancer · Poly(D-glucosamine)/gold nanoparticles/carbon nitride · miRNA-155 · Hairpin electrochemical biosensor · Human serum samples

Introduction

Breast cancer has become one of the most common malignant cancer, with 2.2 million cases per year globally. A large number of studies have proved that miRNAs are closely associated with their occurrence, development, and prognosis [1–3]. MicroRNA (miRNA) is a category of endogenous, non-coding single-stranded small RNA molecules with approximately 20–24 nucleotides that are involved in sorts of physiological and pathological processes [4]. MicroRNA-155 is one of the most widely studied miRNAs, and its high expression in the course of cancer development makes it a novel marker of breast cancer [5–8]. The current main methods to detect miRNA include traditional Northern blotting, microarray, and real-time quantitative PCR, all of which have their advantages. Still, they require expensive equipment and time-consuming experimental process [9–11]. The electrochemical sensors have the superiority of simple equipment, fast response, high sensitivity, and easy operation. They are also capable to achieve sensitive, efficient, and rapid target detections in actual samples or field environments [12–14]. Therefore, the electrochemical sensor

Pingping Peng and Sheng Wang contributed equally to this work.

✉ Nicole Jaffrezic-Renault
nicole.jaffrezic@univ-lyon1.fr

✉ Zhenzhong Guo
zhongbujueqi@hotmail.com

1 Hubei Province Key Laboratory of Occupational Hazard Identification and Control, Wuhan University of Science and Technology, Wuhan 430065, People's Republic of China

2 School of Public Health, Medical College, Wuhan University of Science and Technology, Wuhan 430065, People's Republic of China

3 Department of Neurosurgery, Tongji Hospital, Tongji Medical College, Huazhong University of Science and Technology, Wuhan, China

4 Langfang Normal University, Langfang 065000, China

5 School of Public Health, The Key Laboratory of Environmental Pollution Monitoring and Disease Control, Ministry of Education, Guizhou Medical University, Guiyang 550025, China

6 Institute of Analytical Sciences, University of Lyon, UMR-CNRS 5280, 5, La Doua Street, 69100 Villeurbanne, France

has a tremendous potential for the monitoring of breast cancer marker miRNA-155.

Electrochemical sensors based on different nanomaterials are listed in Table 1. These sensors achieved low detection limits and required relatively complex steps. As one of the essential components of miRNA sensors, hairpin capture probes (HP) were formed when single-stranded DNA molecules met by folding back on themselves, causing complementary base pairs to form hydrogen bonds [21]. Compared with conventional linear nucleic acid molecular probes, DNA probes with hairpin structure can distinguish nucleic acid base pairs well and have higher specificity [22]. Therefore, in the field of miRNA detection, nucleic acid amplification strategies such as strand displacement amplification (SDA) and target-catalyzed hairpin assembly (CHA) based on hairpin structures have been widely used in various biosensors [23, 24]. For example, Zhou et al. used hairpin-type nucleic acid chains as capture probes, combined with a hybridization chain reaction. They introduced CuCo-CeO_2 nanospheres to achieve ultrasensitive electrochemical analysis of miRNA-155 specificity with the detection limit of 0.05 fM, demonstrating the advantages of hairpin-type probes for trace detection of microRNA biomarkers [18]. Therefore, it is valuable to construct a sensitive and straightforward miRNA-155 sensor based on hairpin DNA probe.

The nanostructure of graphite-like carbon nitride (g-C_3N_4) is similar to the two-dimensional planar lamellae of graphene, and the carbon and nitrogen atoms in the structure have formed a highly delocalized π-conjugated system through hybridization [25]. Because of its excellent visible light activity, high specific surface area, and good electrochemical performance, it has caught extensive attention in the professional field of photocatalysis and sensing [26–28]. Gold nanoparticles (NPs) are also widely used in electrochemical sensors on account of their good conductivity, which can significantly enhance the current response signal [29, 30]. The g-C_3N_4 nanosheets were used as carriers and combined with gold nanoparticles through electrostatic adsorption, which can further increase the specific surface area of nanocomposites and promote electron transfer through synergistic effects. Poly(D-glucosamine) (PDG), also known as chitosan, is a biopolymer containing rich active amino and hydroxyl groups obtained by the deacetylation of chitin [31, 32]. Its amino group can be protonated under acidic conditions to obtain cationic polyelectrolyte [33]. In addition, the strong intermolecular hydrogen bonding makes it have good film-forming properties [34, 35]. PDG can also be regarded as a reducing agent and stabilizing agent to synthesize AuNPs at room temperature.

For the study, an electrochemical hairpin biosensor based on PDG/AuNPs/g-C_3N_4 nanocomposite for the miRNA-155 detection was proposed. After the composite material was synthesized at room temperature, and then applied dropwise to cover the surface of the glassy carbon electrode, a conductive film is obtained with an amplifying effect on the electrical signal. Then, the sulfhydryl-modified DNA strand [36] was annealed to obtain an HP through an Au–S bond to connect with the modified electrode to obtain the corresponding hairpin biosensor. When the biomarker miRNA-155 was captured by the HP, the electron transfer reaction on the electrode surface was blocked, and the peak current signal decreased. The hairpin biosensor used differential pulse voltammetry to obtain the calibration curve, and its performance was evaluated, including stability, specificity, and repeatability. Finally, the electrochemical hairpin biosensor was applied for the miRNA detection in actual serum samples of breast cancer patients, indicating its practical significance in early screening and auxiliary diagnosis of breast cancer.

Experiment

Materials and apparatus

The sulfhydryl-modified hairpin probe sequence was synthesized and further purified by Sangon Biotech Co., Ltd. from Shanghai, China, and its modified DNA sequence was 5′-TAA TCG TGA TAG GGG TAT GGA CAT GGA ACC CCT ATC ACG ATT AGC ATT AAA GA-SH-(CH2)6–3′. All of the synthesized and purified RNA sequences were also purchased from Sangon Biotechnology Co. (Shanghai,

Table 1 Comparison with different reported miRNA-155 biosensors

Method	Materials	Linear range	LOD	Ref
Electrochemical	MoS_2	1 fM–10 nM	0.32 fM	[15]
Electrochemical	rGO/poly(2-aminobenzylamine)/AuNPs	1 fM–10 nM	0.98 fM	[16]
Electrochemical	Fc/HGQs/Fe_3O_4	0.1 fM–1 nM	74.8 aM	[17]
Electrochemical	CuCo-CeO_2	0.1 fM–10 nM	0.05 fM	[18]
Electrochemiluminescence	luminol-AuNPs-Ti_3C_2	0.3 fM–1 nM	0.15 fM	[19]
Electrochemiluminescence	Ru-MOF	0.8 fM–1 nM	0.3 fM	[20]
Electrochemical	PDG/AuNPs/g-C_3N_4	0.1 fM–1 pM	0.05 fM	This work

China). HAuCl4·3H2O, PDG, and bovine serum albumin (BSA) were provided by Sigma-Aldrich (St. Louis, Missouri, USA). Graphite-like carbon nitride was purchased from XFNANO Technology Co., Ltd. in Nanjing, China. And the phosphate buffer solution (PBS, 0.1 M pH 7.40) was configurated by KCl, NaCl, Na2HPO4, and KH2PO4. The chemicals mentioned above belong to analytical reagent grade and without further purification. The water used was ultrapure in the whole experiment (conductivity of 18.25 MΩ cm).

Analytical techniques used include electrochemical impedance spectroscopy (EIS) and electrochemical cyclic voltammetry (CV) for characterization. In addition, electrochemical differential pulse voltammetry (DPV) was used for target miRNA detection. These electrochemical analysis methods were performed by using a CS2350H electrochemical workstation which was from Wuhan Corrtest Instrument (Wuhan, China). A traditional three-electrode system was used, with a 3 mm diameter glassy carbon working electrode (GCE), a saturated Ag/AgCl reference electrode, and a platinum wire counter electrode. 5 mM concentration [Fe $(CN)_6]^{3-}$/[Fe $(CN)_6]^{4-}$ redox in PBS (pH 7.40) was used as the electrolyte solution for electrochemical analysis. Transmission electron microscopy was used to characterize the structure and morphology of the synthesized composites (TEM, Tecnai G2 F30).

Synthesis of PDG/AuNPs/g-C_3N_4 nanocomposites

AuNPs were synthesized using PDG reduced under room temperature through the magnetic stirring method. The specific procedure was as follows: 50 mg of PDG powder was dissolved in 10 mL 1% dilute acetic acid solution and stirred magnetically for 30 min to obtain a clear and transparent mixture. Then the $HAuCl_4{\cdot}3H_2O$ solution with the concentration of 0.01 M, 200 µL was slowly added to the above precursor solution and stirred continuously at a magnetic stirring speed of 750 rpm under room temperature. After continuous stirring for 4 h, the color of the reaction solution changed from light yellow to faint red, indicating that PDG/AuNPs were successfully synthesized and stored in the refrigerator at 4 °C. The synthesis steps of PDG/AuNPs/g-C_3N_4 composites were as follows. Firstly, bulk g-C_3N_4 nanosheets need to be exfoliated by ultrasonication. Briefly, a g-C_3N_4 solution with the concentration of 1 mg mL^{-1} was sonicated continuously for 4 h. Subsequently, the solution was centrifuged at 2000 rpm for 20 min, and the liquid supernatant was collected to obtain a g-C_3N_4 nanosuspension. Then 100 µL of g-C_3N_4 nanosuspension was aspirated and added to 150 µL of PDG/AuNPs solution, following the mixture was sonicated for 30 min to obtain a homogeneous mixed solution. Finally, the PDG/AuNPs/g-C_3N_4 nanocomposite was stored in a refrigerator at 4 °C for later use.

Analytical procedure

In this experiment, the glassy carbon electrodes were polished to the mirror surface using 0.3 µm and 0.05 µm alumina powder one after another. Then the electrodes were ultrasonically cleaned in ethyl alcohol and ultrapure water each for 5 min, and activated by electrochemical cleaning in a 0.5 M sulfuric acid solution. After each step, the electrodes were rinsed repeatedly with ultrapure water, and eventually, the electrodes were dried in a constant temperature drying oven at 50 °C after activation.

After preprocessing the electrode, the modified electrode was obtained by dropping 6 µL of nanocomposite suspension liquid on the clean surface of the GCE and then drying it. The DNA sequence was heated to 95 °C, annealed for 2 min, and cooled down to room temperature, and then HP was obtained. 6 µL of 1.5 µM HP solution was dropwise deposited on the nanocomposite modified GCE surface and incubated at 4 °C for 14 h in the refrigerator. Subsequently, the non-specific binding sites were passivated using 6 µL of 0.25% BSA solution at 37 °C for 30 min, followed by PBS (pH 7.40) washing. Finally, drying under nitrogen was carried out, and 6 µL of different concentrations of the miRNA-155 solutions were added to the electrode surface and subsequently incubated at 37 °C for 45 min before recording the current signal values by the DPV method, in the presence of 5 mM redox probe.

Collected actual serum samples

The human serum samples were collected from China Resources & Wisco General Hospital. All samples were conformed to the Helsinki Declaration and approved by the Ethics Committee and the consent of informed volunteers. The fasting venous blood was collected in anticoagulation tubes, centrifuged (4 °C, 15 min, 3000 rpm), and following the supernatant was taken to obtain serum samples, which were stored at − 80 °C for testing.

Results and discussion

Sensing scheme

For this study, an ultrasensitive biosensor based on g-C_3N_4, PDG, and gold nanoparticle nanocomposite was proposed, for the detection of miRNA-155. As shown in Scheme 1, PDG contains a mass of hydroxyl groups and -NH_3^+ under acidic conditions, which can be used as a stabilizer and reducing agent to prepare gold nanoparticles with tetrachloride acid as raw material. While g-C_3N_4 was a two-dimensional nanosheet with a lamellar structure and it was exfoliated under ultrasonication, the specific surface area

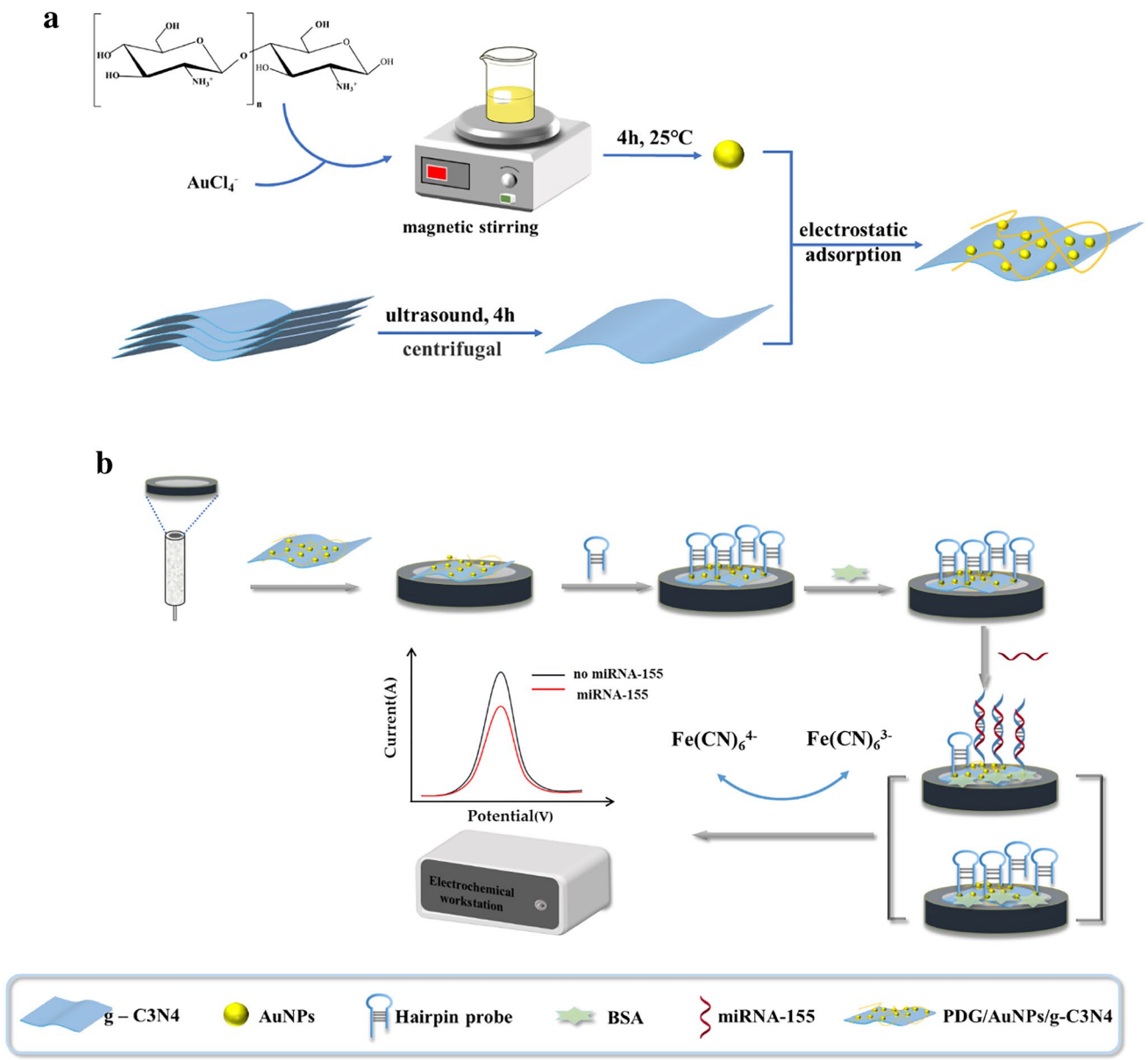

Scheme 1 Fabrication of the sensing platform

was then increased to be used as a carrier to provide abundant gold nanoparticle attachment sites. The PDG/AuNPs/g-C_3N_4 composites were synthesized by combining g-C_3N_4 with PDG/AuNPs via electrostatic adsorption. When the compound was applied to the surface of the GCE electrode, a conductive film coating was formed to significantly enhance the current signal value and improve the sensitivity of the sensor. The miRNA-155 could be specifically recognized after the HP was incubated on the surface of the modified electrode. The presence of miRNA-155 would lead to the change in the current signal. In the absence of miRNA-155, the electron transfer on the immune electrode surface was not hindered, and the redox reaction could proceed faster. When miRNA-155 is present, the electron transfer rate was affected by its electronegativity due to the appearance of a DNA-RNA hybrid double strand, and the electrical signal recorded by the electrochemical workstation subsequently decreases. Finally, the hairpin biosensor proposed in this study has been applied to detect miRNA-155 in human serum.

Morphology and structure characterization

As shown in Fig. 1, in order to characterize the nanomaterials, transmission electron microscopy (TEM) was used for observation analysis of their morphologies

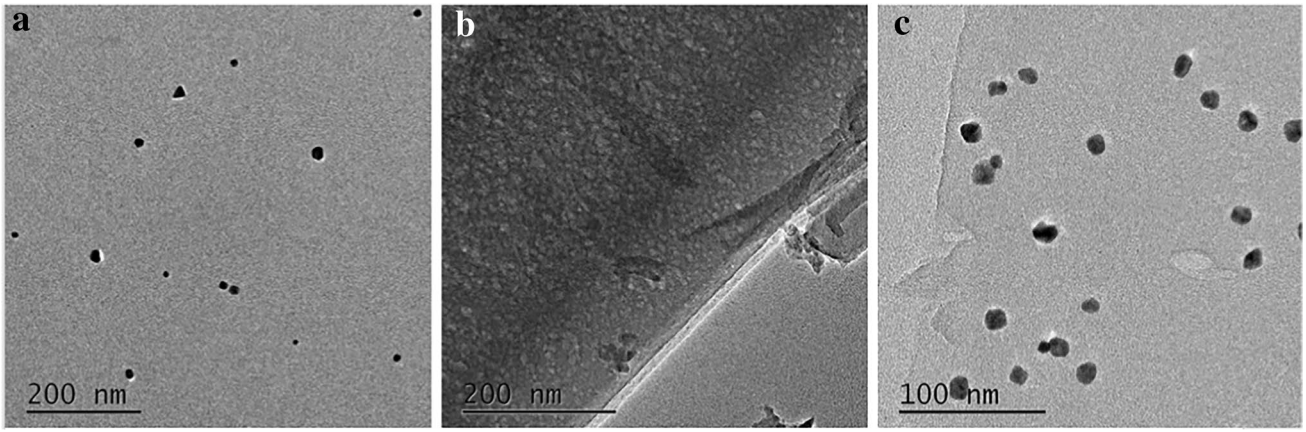

Fig. 1 TEM image of the **a** PDG/AuNPs, **b** g-C_3N_4, **c** PDG/AuNPs/g-C_3N_4

and structures. Figure 1a shows the gold nanoparticles obtained after the reduction of gold tetrachloride acid, indicating that they can be successfully synthesized using PDG at room temperature. The uniformly dispersed gold nanoparticles with a particle size of approximately 12 nm are observed in Fig. 1a. In Fig. 1b, the thin layer of g-C_3N_4 spreads in a flake shape, manifesting that the large g-C_3N_4 nanolayers were successfully exfoliated. In addition, Fig. 1c shows the TEM diagram of PDG/AuNPs/g-C_3N_4 composite material that gold nanoparticles were uniformly adsorbed on the surface of the g-C_3N_4 nanosheet. They form composites by electrostatic adsorption and have the potential to significantly increase the current signal response value by synergistically achieving an increase in electrical conductivity and specific surface area.

Electrochemical characterization of the hairpin biosensor

CV and EIS were essential methods for the electrochemical characterization of hairpin biosensors. It can be seen from Fig. 2a that the changes in the redox current value of CV correspond to each step of the modification process of the GCE electrode. The bare GCE (curve a, black) presents the smallest current value, and the current signal value of the modified electrode was significantly higher after the dropwise addition of PDG/AuNPs complexes (curve b, red). It was account of the satisfactory electrical conductivity of gold nanoparticles and high specific surface area, which expedited the electron transfer rate of the redox probe [Fe $(CN)_6]^{3-/4-}$]. The redox current value (curve c, blue) was further increased after the addition of g-C_3N_4, which was

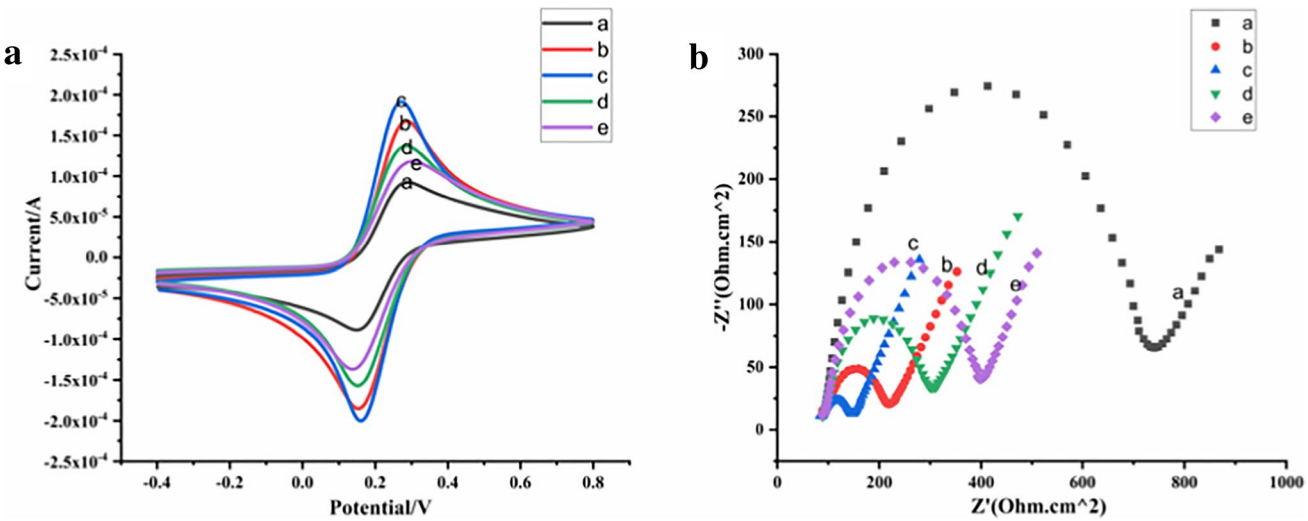

Fig. 2 The CV (**a**) and EIS (**b**) electrochemical characterization of biosensor platform fabrication. (a) bare/GCE; (b) PDG/AuNPs/GCE; (c) PDG/AuNPs/g-C_3N_4/GCE; (d) PDG/AuNPs/g-C_3N_4/HP/GCE; (e) PDG/AuNPs/g-C_3N_4/HP/miRNA-155/GCE

ascribed to the laminar structure of g-C_3N_4 further increasing the surface area to accelerate the electron transfer reaction. After incubation of the HP overnight (curve d, green), the signal value decreased significantly. After miRNA-155 was captured by the hairpin sequence (curve e, purple), the signal was further attenuated. It was because DNA probes and RNA sequences had a large number of phosphate groups and were negatively charged, resulting in electrostatic repulsion that impeded the electron transfer rate. CV characterization results indicated the successful construction of a miRNA-155 hairpin-based electrochemical biosensor.

In Fig. 2b, the hairpin sensor was characterized by EIS, and the diameter of the high-frequency half-arc of the Nyquist plot represented the magnitude of the electron transfer resistance on the corresponding electrode surface. Obviously, the highest impedance of the bare electrode in the figure (curve a, black) was about 600 Ohm. After modification by PDG/AuNPs, the semicircle diameter of curve b (red) was greatly reduced to about 133 Ohm, its good electrical conductivity. After further modification of PDG/AuNPs/g-C_3N_4, the semicircle size of curve c (blue) was further reduced (67 Ohm), indicating that the addition of g-C_3N_4 enhanced the specific surface area of the composite and accelerated the electron transfer rate. Curves d (green) and e (purple) represent the impedance values of the capture probe (200 Ohm) and the eventual incubation of miRNA-155 (316 Ohm) on the modified electrode surface of the composite, respectively. The semicircle diameter of curves d and curves e increased successively from Fig. 2b, because of the negative charges of the nucleic acid sequence that led to the increase of resistance value. The above results were in accord with the characterization by CV, which demonstrated the successful construction of the sensor.

Optimization of experimental conditions

Experimental conditions affecting the result data were optimized to improve the performance of the sensing platform. The peak current values for condition optimization were measured by the DPV method, and the current difference $\Delta I = I_p - I_0$ (I_p: response value in the presence of miRNA-155, I_0: response value in the absence of miRNA-155) was measured. The optimization of the HP concentration is shown in Fig. S1(a). It is clear that the difference increased when the concentration increases from 0.5 to 1.5 μM, after which the difference decreased as the concentration increases, indicating that the active sites tend to saturate. From the figure, it can be seen that the optimal concentration of the HP was 1.5 μM.

The incubation time of the HP was also one of the factors affecting the sensor performance. The DPV current difference in Fig. S1(b) shows that the difference was the largest when the incubation time with the capture probe is 14 h. All subsequent experiments were carried out under the condition of incubating the capture probe for 14 h.

In Fig. S1(c), the current difference varies with the volume of PDG/AuNPs/g-C_3N_4 suspension, on account of the thickness of the coating film for the composite onto the electrode affects electron transfer. When the volume of the coating film was less than 6 μL, the current difference increased with the volume of the material. On the other hand, when the volume was larger than 6 μL, the thick nanocoating blocked electron transfer and current difference shows a decreasing trend. It could be concluded that the experimental conditions were optimal when the volume of coated film of PDG/AuNPs/g-C_3N_4 composite on the electrode surface was 6 μL.

Quantification of miRNA-155 in PBS

The miRNA-155 standard curves were all measured under the optimal experimental conditions, and the correlation between the concentration of the target and the peak current value was analyzed using the DPV method. From the analysis in Fig. 3a, it can be obtained that in the range of 0.1 fM–1 pM, when the concentration of the miRNA-155 standard solution increases, the DPV peak current shows a decreasing trend. It is because significantly more miRNA-155 has formed a negatively charged complex with the HP, the electron transfer was impeded and the reaction rate of [Fe(CN)6]$^{3-/4-}$] reduced, and the current decreased accordingly.

In Fig. 3b, it can be clearly seen that the logC value of the miRNA-155 standard solution has shown a linear trend with the DPV redox peak value difference ΔI ($I_p - I_0$, I_p: the current response value of miRNA-155, I_0: the current response value of blank). In addition, the linear regression equation between the two variables was $\Delta I = 6.141 \log C + 115.186$ (C: the concentration of 10^{-16}–10^{-12} mol L^{-1} for miRNA-155), and the correlation coefficient (R^2) was 0.996. According to the standard curve and the relevant provisions of the International Union of Pure and Applied Chemistry (IUPAC), the LOD value was determined as $3\sigma/S$, σ being the background of the blank and S the sensitivity to be equal to 0.05 fM [37]. This detection limit is very low, compared to that of the previously published miRNA-155 electrochemical biosensors (Table 1). The ultrasensitive analysis of the biosensing platform for miRNA-155 was demonstrated.

Quantitation of miRNA-155 in serum

To further investigate the practical application potential of this hairpin biosensor in the detection of miRNA-155 in actual serum samples, a series of miRNA-155 solutions with healthy human serum diluted at a ratio of 1:4000 was configured, and the concentration gradient is shown in Fig. S2. The solution concentration was configured with five

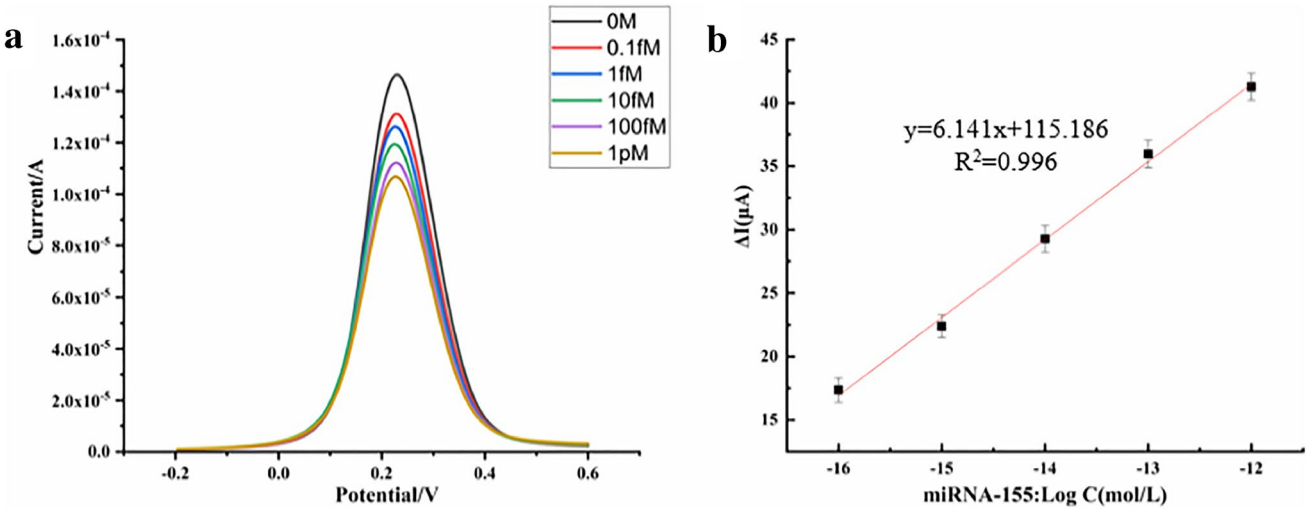

Fig. 3 **a** DPV current responses for different miRNA-155 concentrations: 10^{-16}, 10^{-15}, 10^{-14}, 10^{-13}, 10^{-12} mol L^{-1}; **b** the calibrated curve of the hairpin type electrochemical biosensor toward different concentrations of miRNA-155

gradients, 10^{-12}, 10^{-13}, 10^{-14}, 10^{-15}, and 10^{-16} mol L^{-1}, in which the DPV current changes were consistent with the standard curve, and the current peak decreased with the increase of miRNA-155 concentration, presented a negative correlation, as shown in Fig. S2(a). In Fig. S2(b), when the sensor worked in human diluted serum, the linear regression equation between the difference of current value and the concentration of the target substance was $\Delta I = 5.578 \log C + 106.471$. Compared with the standard curve, the correlation coefficient R^2 was 0.991, less than 0.996, which was decreased because the serum matrix is more complex, which affects the linear relationship. However, the above data results all met the requirements, indicating that the sensor could be applied to the miRNA-155 detection in actual serum samples within the concentration range from 10^{-16} to 10^{-12} mol L^{-1}.

Selectivity, reproducibility, and stability of biosensor

In this study, several interfering RNAs were selected to confirm the specificity of the miRNA-155 hairpin sensor, including miRNA-141, miRNA-21, miRNA-210, and let-7a [38, 39], which have partially identical base sequences with the target RNA (Table S1). The concentration of interfering RNA was 100 times more than that of the miRNA-155, and the concentration of miRNA-155 was 10^{-14} mol L^{-1}. As shown in Fig. 4a, when the interference concentration was much higher than that of miRNA-155, the DPV current difference of miRNA-155 was still significantly higher than that of interfering miRNA, and the interfering RNA concentration was all lower than 10 μA. Therefore, the miRNA-155 hairpin biosensor proposed in

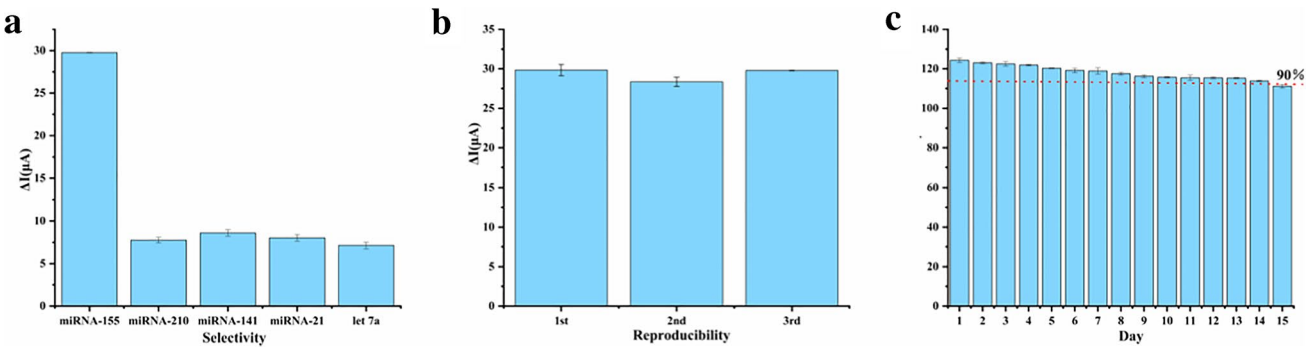

Fig. 4 **a** Selectivity of the hairpin electrochemical biosensor. The concentration of interfering RNA was 100 times more than that of the miRNA-155, and the concentration of miRNA-155 was 10^{-14} mol L^{-1}; **b** reproducibility of three different hairpin biosensors; **c** stability of the PDG/AuNPs/g-C_3N_4 based hairpin biosensor stored at 4 °C

this study had a good selectivity and could be applied to serum samples with the complex matrix.

Regarding the reproducibility performance assessment of the sensor, three electrodes were established in the same experimental operation method, and the identical concentration of miRNA-155 solution was measured by DPV method. The measurement results showed (Fig. 4b) that the DPV current difference values of all three electrodes were less than 5%. This result indicates that the hairpin biosensor had a good reproducibility.

Stability is also one of the critical properties belonging to the sensor, and the same conditions were used throughout the experiments. The constructed hairpin electrochemical biosensor was assayed for a certain concentration of miRNA-155 and stored in a 4 °C refrigerator. The treated electrodes were measured daily for 15 days. Some information can be seen in Fig. 4c, and the DPV current value on the 15th day was more than 90% of that on the first day, indicating that the electrochemical sensor had a good stability.

Actual serum sample measurement

The above results demonstrated the good performance of the hairpin electrochemical biosensor proposed in this study, so spiked recovery experiments were performed in 4000 times diluted serum of healthy humans, as shown in Table 2. After the addition of the corresponding miRNA-155 solution, the spiked recoveries were 101.16%, 102.57%, and 97.17% after three measurements on average, with the corresponding relative standard deviations (RSDs) of 2.85%, 2.11%, and 3.21%, respectively. The above data suggested that the sensor had the potential to be applied for the miRNA-155 detection in actual serum samples. Therefore, in this study, serum from two healthy individuals, two cured patients, and six breast cancer patients were collected and studied for preliminary detection using this sensor (Fig. 5). The results have revealed that miRNA-155, a breast cancer biomarker that changes accordingly during the progression of the disease, was significantly higher in the serum of breast cancer patients than in other subjects. The ultrasensitive detection of miRNA-155 in serum by this sensor indicates its potential for clinical application and early diagnosis.

Table 2 Recovery of miRNA-155 in healthy human serum samples

Sample	Added (fM)	Found (fM)	Recovery (%)	RSDs (%)
1	5	5.058	101.16	2.85
2	50	51.286	102.57	2.11
3	500	485.870	97.17	3.21

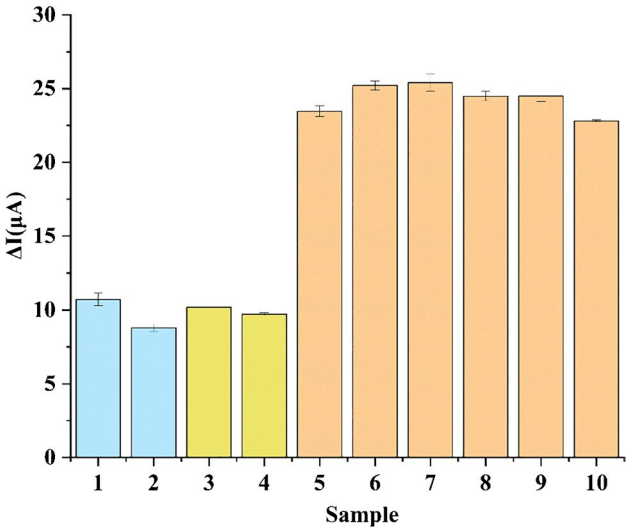

Fig. 5 The difference of healthy (blue), post-cured humans (yellow), and breast cancer patients (orange)

Conclusions

As PDG contains a large amount of polycationic NH_3^+ under acidic conditions, gold nanoparticles could be successfully synthesized under the condition of normal temperature magnetic agitation and then combined with a g-C_3N_4 carrier, PDG/AuNPs/g-C_3N_4 composite with excellent amplification of electrical signals could be obtained. The hairpin electrochemical biosensor based on composite materials had a wide detection range for miRNA-155, and the detection limit was as low as 0.05 fM. In addition, the accuracy, stability, specificity, and reproducibility of the sensor showed good experimental results, and further analyses of miRNA-155 in actual human serum samples were performed. Therefore, the PDG/AuNPs/g-C_3N_4 hairpin sensor has a particular practical analysis for miRNA-155, which is conducive to the early detection of breast cancer patients and provides a new therapeutic monitoring approach for the corresponding diagnosis.

Supplementary Information The online version contains supplementary material available at https://doi.org/10.1007/s00216-022-04284-0.

Author contribution PP: writing—original draft, conceptualization, software. SW: software, resources. SC: software. JC: software. DT: funding acquisition. NJ-R: funding acquisition, writing—reviewing and editing. ZG: funding acquisition, conceptualization, project administration, supervision.

Funding This work was supported by National Natural Science Foundation of China (No. 81973097), Key Research and Development Project of Hubei Province (No. 2020BCB022), Outstanding Young and Middle-Aged Technology Innovation Team Project of Hubei Provincial Department of Education (No. T2020003), Opening Fund of State Key Laboratory of Wuhan University (No. 2022KF002), Opening Project

of Key Laboratory of Optoelectronic Chemical Materials and Devices of Ministry of Education of Jianghan University (No. JDGD-202018), Doctoral Startup Foundation of Guizhou Medical University (grant no. J[2021]063), and CNRS France is acknowledged for support through IRN MAREES # 0876.

Declarations

Ethics approval All samples were conformed to the Helsinki Declaration and approved by the Ethics Committee of China Resources & Wisco General Hospital and Wuhan University of Science and Technology.

Conflict of interest The authors declare no competing interests.

References

1. Mulrane L, McGee SF, Gallagher WM, O'Connor DP. miRNA dysregulation in breast cancer. Cancer Res. 2013;73(22):6554–62. https://doi.org/10.1158/0008-5472.CAN-13-1841.
2. Ansari MA, Thiruvengadam M, Farooqui Z, Rajakumar G, Sajid Jamal QM, Alzohairy MA, et al. Nanotechnology, in silico and endocrine-based strategy for delivering paclitaxel and miRNA: prospects for the therapeutic management of breast cancer. Semin Cancer Biol. 2021;69:109–28. https://doi.org/10.1016/j.semcancer.2019.12.022.
3. Crudele F, Bianchi N, Reali E, Galasso M, Agnoletto C, Volinia S. The network of non-coding RNAs and their molecular targets in breast cancer. Mol Cancer. 2020;19(1):61. https://doi.org/10.1186/s12943-020-01181-x.
4. Mori MA, Ludwig RG, Garcia-Martin R, Brandao BB, Kahn CR. Extracellular miRNAs: from biomarkers to mediators of physiology and disease. Cell Metab. 2019;30(4):656–73. https://doi.org/10.1016/j.cmet.2019.07.011.
5. Rodriguez-Martinez A, de Miguel-Perez D, Ortega FG, Garcia-Puche JL, Robles-Fernandez I, Exposito J, et al. Exosomal miRNA profile as complementary tool in the diagnostic and prediction of treatment response in localized breast cancer under neoadjuvant chemotherapy. Breast Cancer Res. 2019;21(1):21. https://doi.org/10.1186/s13058-019-1109-0.
6. Kong W, He L, Richards EJ, Challa S, Xu CX, Permuth-Wey J, et al. Upregulation of miRNA-155 promotes tumour angiogenesis by targeting VHL and is associated with poor prognosis and triple-negative breast cancer. Oncogene. 2014;33(6):679–89. https://doi.org/10.1038/onc.2012.636.
7. Swellam M, Ramadan A, El-Hussieny EA, Bakr NM, Hassan NM, Sobeih ME, et al. Clinical significance of blood-based miRNAs as diagnostic and prognostic nucleic acid markers in breast cancer: comparative to conventional tumor markers. J Cell Biochem. 2019;120(8):12321–30. https://doi.org/10.1002/jcb.28496.
8. McDonald SJ, Cranford TL, Cranford BN, Cranford T, Fan DP, Cranford AE. Role of miRNA-155 on tumorigenesis in a transgenic mouse model of breast cancer. FASEB J. 2022;36:R01CA218578-03S1. https://doi.org/10.1096/fasebj.2022.36.S1.L7839.
9. Varallyay E, Burgyan J, Havelda Z. MicroRNA detection by northern blotting using locked nucleic acid probes. Nat Protoc. 2008;3(2):190–6. https://doi.org/10.1038/nprot.2007.528.
10. Liu CG, Calin GA, Volinia S, Croce CM. MicroRNA expression profiling using microarrays. Nat Protoc. 2008;3(4):563–78. https://doi.org/10.1038/nprot.2008.14.
11. Kang K, Peng X, Luo J, Gou D. Identification of circulating miRNA biomarkers based on global quantitative real-time PCR profiling. J Anim Sci Biotechnol. 2012;3(1):4. https://doi.org/10.1186/2049-1891-3-4.
12. Masud MK, Umer M, Hossain MSA, Yamauchi Y, Nguyen NT, Shiddiky MJA. Nanoarchitecture frameworks for electrochemical miRNA detection. Trends Biochem Sci. 2019;44(5):433–52. https://doi.org/10.1016/j.tibs.2018.11.012.
13. Tran HV, Piro B. Recent trends in application of nanomaterials for the development of electrochemical microRNA biosensors. Mikrochim Acta. 2021;188(4):128. https://doi.org/10.1007/s00604-021-04784-3.
14. Singh P, Pandey SK, Singh J, Srivastava S, Sachan S, Singh SK. Biomedical perspective of electrochemical nanobiosensor. Nanomicro Lett. 2016;8(3):193–203. https://doi.org/10.1007/s40820-015-0077-x.
15. Liu L, Zhu S, Wei Y, Liu X, Jiao S, Yang J. Ultrasensitive detection of miRNA-155 based on controlled fabrication of AuNPs@MoS2 nanostructures by atomic layer deposition. Biosens Bioelectron. 2019;144: 111660. https://doi.org/10.1016/j.bios.2019.111660.
16. Pimalai D, Putnin T, Waiwinya W, Chotsuwan C, Aroonyadet N, Japrung D. Development of electrochemical biosensors for simultaneous multiplex detection of microRNA for breast cancer screening. Mikrochim Acta. 2021;188(10):329. https://doi.org/10.1007/s00604-021-04995-8.
17. Zhu L, Zhang X, Chang Y, Xu S, Yuan R, Chai Y. Co-catalytic Fc/HGQs/Fe3O4 nanocomposite mediated enzyme-free electrochemical biosensor for ultrasensitive detection of microRNA. Chem Commun (Camb). 2021;57(42):5179–82. https://doi.org/10.1039/D1CC01106E.
18. Zhou C, Cui K, Liu Y, Li L, Zhang L, Xu M, et al. Ultrasensitive lab-on-paper device via Cu/Co double-doped CeO2 nanospheres as signal amplifiers for electrochemical/visual sensing of miRNA-155. Sensors Actuators B Chem. 2020;321: 128499. https://doi.org/10.1016/j.snb.2020.128499.
19. Zhuang T, Zhang H, Wang L, Yu L, Wang Z. Anchoring luminol based on Ti3C2-mediated in situ formation of Au NPs for construction of an efficient probe for miRNA electrogenerated chemiluminescence detection. Anal Bioanal Chem. 2021;413(28):6963–71. https://doi.org/10.1007/s00216-021-03651-7.
20. Jian Y, Wang H, Lan F, Liang L, Ren N, Liu H, et al. Electrochemiluminescence based detection of microRNA by applying an amplification strategy and Hg(II)-triggered disassembly of a metal organic frameworks functionalized with ruthenium(II) tris(bipyridine). Mikrochim Acta. 2018;185(2):133. https://doi.org/10.1007/s00604-018-2693-x.
21. Henderson E, Hardin CC, Walk SK, Tinoco I Jr, Blackburn EH. Telomeric DNA oligonucleotides form novel intramolecular structures containing guanine-guanine base pairs. Cell. 1987;51(6):899–908. https://doi.org/10.1016/0092-8674(87)90577-0.
22. Hakimian F, Ghourchian H. Ultrasensitive electrochemical biosensor for detection of microRNA-155 as a breast cancer risk factor. Anal Chim Acta. 2020;1136:1–8. https://doi.org/10.1016/j.aca.2020.08.039.
23. Zhang P, Liu H, Li X, Ma S, Men S, Wei H, et al. A label-free fluorescent direct detection of live Salmonella typhimurium using cascade triple trigger sequences-regenerated strand displacement amplification and hairpin template-generated-scaffolded silver nanoclusters. Biosens Bioelectron. 2017;87:1044–9. https://doi.org/10.1016/j.bios.2016.09.037.
24. Zhu MH, Mu XM, Deng HM, Zhong X, Yuan R, Yuan YL. Ultrasensitive photoelectrochemical biosensor for MiRNA-21 assay based on target-catalyzed hairpin assembly coupled with distance-controllable multiple signal amplification. Chem Commun

(Camb). 2019;55(65):9622–5. https://doi.org/10.1039/C9CC04987H.
25. Niu P, Zhang L, Liu G, Cheng H-M. Graphene-like carbon nitride nanosheets for improved photocatalytic activities. Adv Funct Mater. 2012;22(22):4763–70. https://doi.org/10.1002/adfm.201200922.
26. Ni Y, Wang R, Zhang W, Shi S, Zhu W, Liu M, et al. Graphitic carbon nitride (g-C3N4)-based nanostructured materials for photodynamic inactivation: synthesis, efficacy and mechanism. Chem Eng J. 2021;404: 126528. https://doi.org/10.1016/j.cej.2020.126528.
27. Shwetharani R, Kapse S, Thapa R, Nagaraju DH, Balakrishna RG. Dendritic ferroselite (FeSe2) with 2D carbon-based nanosheets of rGO and g-C3N4 as efficient catalysts for electrochemical hydrogen evolution. ACS Appl Energ Mater. 2020;3(12):12682–91. https://doi.org/10.1021/acsaem.0c02619.
28. Liu L, Wang M, Wang C. In-situ synthesis of graphitic carbon nitride/iron oxide–copper composites and their application in the electrochemical detection of glucose. Electrochim Acta. 2018;265:275–83. https://doi.org/10.1016/j.electacta.2018.01.149.
29. Wei X, Duan X, Zhou X, Wu J, Xu H, Min X, et al. A highly sensitive SPRi biosensing strategy for simultaneous detection of multiplex miRNAs based on strand displacement amplification and AuNP signal enhancement. Analyst. 2018;143(13):3134–40. https://doi.org/10.1039/C8AN00549D.
30. Kolzunova L, Shchitovskaya E, Karpenko M. Polymethylolacrylamide/AuNPs nanocomposites: electrochemical synthesis and functional characteristics. Polymers (Basel). 2021;13(14):2382. https://doi.org/10.3390/polym13142382.
31. Dash M, Chiellini F, Ottenbrite RM, Chiellini E. Chitosan—a versatile semi-synthetic polymer in biomedical applications. Prog Polym Sci. 2011;36(8):981–1014. https://doi.org/10.1016/j.progpolymsci.2011.02.001.
32. Figiela M, Wysokowski M, Galinski M, Jesionowski T, Stepniak I. Synthesis and characterization of novel copper oxide-chitosan nanocomposites for non-enzymatic glucose sensing. Sensors Actuators B Chem. 2018;272:296–307. https://doi.org/10.1016/j.snb.2018.05.173.
33. Dey A, Kamat A, Nayak S, Danino D, Kesselman E, Dandekar P, et al. Role of proton balance in formation of self-assembled chitosan nanoparticles. Colloid Surface B. 2018;166:127–34. https://doi.org/10.1016/j.colsurfb.2018.03.017.
34. Liu XP, Huang B, Mao CJ, Chen JS, Jin BK. Electrochemiluminescence aptasensor for lincomycin antigen detection by using a SnO2/chitosan/g-C3N4 nanocomposite. Talanta. 2021;233:122546. https://doi.org/10.1016/j.talanta.2021.122546.
35. Magerusan L, Pogacean F, Coros M, Socaci C, Pruneanu S, Leostean C, et al. Green methodology for the preparation of chitosan/graphene nanomaterial through electrochemical exfoliation and its applicability in Sunset Yellow detection. Electrochim Acta. 2018;283:578–89. https://doi.org/10.1016/j.electacta.2018.06.203.
36. Wang H, Jian Y, Kong Q, Liu H, Lan F, Liang L, et al. Ultrasensitive electrochemical paper-based biosensor for microRNA via strand displacement reaction and metal-organic frameworks. Sensors Actuators B Chem. 2018;257:561–9. https://doi.org/10.1016/j.snb.2017.10.188.
37. Burgues J, Jimenez-Soto JM, Marco S. Estimation of the limit of detection in semiconductor gas sensors through linearized calibration models. Anal Chim Acta. 2018;1013:13–25. https://doi.org/10.1016/j.aca.2018.01.062.
38. Liu D, Yang G, Zhang X, Chen S, Yuan R. A novel potential-regulated ratiometric electrochemiluminescence sensing strategy based on poly(9,9-di-n-octylfluorenyl-2,7-diyl) polymer nanoparticles for microRNA detection. Sensors Actuators B Chem. 2021;329: 129210. https://doi.org/10.1016/j.snb.2020.129210.
39. Wang F, Fu C, Huang C, Li N, Wang Y, Ge S, et al. Paper-based closed Au-bipolar electrode electrochemiluminescence sensing platform for the detection of miRNA-155. Biosens Bioelectron. 2020;150: 111917. https://doi.org/10.1016/j.bios.2019.111917.